Biomaterials Science

PAPER

View Article Online
View Journal | View Issue

Cite this: *Biomater. Sci.*, 2020, **8**, 278

Antibacterial and hydroxyapatite-forming coating for biomedical implants based on polypeptide-functionalized titania nanospikes†

Qiang Gao,[a,b] Tao Feng,[c] Danni Huang,[a] Peng Liu,[d] Peng Lin,[e] Yan Wu,[e] Zhaoming Ye,[e] Jian Ji, *[a] Peng Li *[c,f] and Wei Huang[c,f]

Titanium (Ti)-based implants often suffer from detrimental bacterial adhesion and inefficient healing, so it is crucial to design a dual-functional coating that prevents bacterial infection and enhances bioactivity for a successful implant. Herein, we successfully devised a cationic polypeptide (Pep)-functionalized biomimetic nanostructure coating with superior activity, which could not only kill pathogenic bacteria rapidly and inhibit biofilm formation for up to two weeks, but also promote *in situ* hydroxyapatite (HAp) formation. Specifically, a titania (TiO_2) nanospike coating (TNC) was fabricated by alkaline hydrothermal treatment firstly, followed by immobilization of rationally synthesized Pep *via* robust coordinative interactions, named TNPC. This coating was able to effectively kill (>99.9%) both Gram-positive *Staphylococcus aureus* (*S. aureus*) and Gram-negative *Escherichia coli* (*E. coli*) bacteria, while being non-toxic to murine MC3T3-E1 osteoblastic cells. Furthermore, the *in vivo* infection studies denoted that the adherent bacteria numbers on the TNPC implants were significantly reduced by 6 orders of magnitude than those on the pure Ti implants ($p < 0.001$). Importantly, in the presence of cationic amino groups and residual Ti-OH groups, substantial HAp deposition on the TNPC surface in Kokubo's simulated body fluid (SBF) occurred after 14 days. Altogether, our results support the clinical potential of this biomimetic dual-functional coating as a new approach with desirable antibacterial properties and HAp-forming ability in orthopedic and dental applications.

Received 1st September 2019,
Accepted 12th October 2019

DOI: 10.1039/c9bm01396b

rsc.li/biomaterials-science

1. Introduction

Titanium (Ti) and its alloys are the preferred selection for clinical implant applications (such as dental implants, artificial joints, heart stents and pacemakers, *etc.*) owing to their excellent corrosion resistance, biocompatibility and non-magnetism.[1,2] Despite such superiorities, some fundamental limitations of Ti-based implants, including early pathogenic bacteria adhesion and subsequent biofilm formation on the implant surface, and poor bioactivity at the bone-implant interface,[3,4] are still the prevailing problems, resulting in serious pain and economic burden for the patients.[5,6] In view of the fact that it is not enough to prepare a single functional surface for infection prevention or bioactivity enhancement, the development of advanced implant coatings with simultaneous antibacterial and biological activities is greatly desired to overcome the above-mentioned problems.[7–9]

Recently, inspired by natural high aspect ratio surface nanotopographies (*e.g.*, cicada/dragonfly wings,[10,11] moth eyes[12] and gecko skin[13]) with antifouling performance by rupturing bacterial membranes, researchers have paid great attention to imitate these nanostructures for developing a new generation of mechano-bactericidal materials.[14–16] Ivanova *et al.* demonstrated that cicada wing nanopillars were effective at killing Gram-negative *Pseudomonas aeruginosa* (*P. aeruginosa*) on contact due to a physico-mechanical effect.[17] Similarly, Watson

[a]*MOE Key Laboratory of Macromolecule Synthesis and Functionalization, Department of Polymer Science and Engineering, Zhejiang University, Hangzhou 310027, China. E-mail: jijian@zju.edu.cn; Fax: +86-571-87963729; Tel: +86-571-87963729*
[b]*Center for Biomedical Engineering and Regenerative Medicine, Frontier Institute of Science and Technology, Xi'an Jiaotong University, Xi'an 710049, China*
[c]*Xi'an Institute of Flexible Electronics & Xi'an Institute of Biomedical Materials and Engineering, Northwestern Polytechnical University (NPU), 127 West Youyi Road, Xi'an 710072, China. E-mail: iampli@nwpu.edu.cn; Fax: +86-29-88492151; Tel: +86-29-88492151*
[d]*Key Laboratory of Biorheological Science and Technology of Ministry of Education, College of Bioengineering, Chongqing University, Chongqing 400044, China*
[e]*Department of Orthopaedics, The Second Affiliated Hospital of Zhejiang University School of Medicine, Hangzhou 310009, China*
[f]*Key Laboratory of Flexible Electronics (KLOFE), Institute of Advanced Materials (IAM), Jiangsu National Synergetic Innovation Center for Advanced Materials (SICAM), Nanjing Tech University, Nanjing 211816, China*
†Electronic supplementary information (ESI) available. See DOI: 10.1039/c9bm01396b

et al. found that gecko skin nanospinules induce the death of Gram-negative *Porphyromonas gingivalis* (*P. gingivalis*) on contact.[13] A variety of synthetic materials have been prepared to mimic these nanotopographies and then bactericidal function was obtained, such as reactive ion etched black silicon,[18] polymer/diamond nanocone arrays,[19,20] nanoimprinted plastics[21,22] and surface attached nanocrystals,[23,24] *etc*. Although these nanostructured surfaces are able to kill Gram-negative bacteria efficiently, their efficiency is poor in the eradication of Gram-positive bacteria (*e.g.*, *Bacillus subtilis, Planococcus maritimus* and *S. aureus*).[25,26] Aside from that, dragonfly wings exhibit non-selective bactericidal activity towards both Gram-negative and Gram-positive bacteria,[11] and the majority of its synthetic analogues are also less effective against Gram-positive bacteria.[15] For biomedical applications, a surface with potent and broad-spectrum antibacterial efficacy against both Gram-negative and Gram-positive bacteria is highly desirable.

In our previous studies, several coatings with potent broad-spectrum antibacterial efficacy were prepared by the surface-initiated radical polymerization of cationic polypeptides (Pep)/polymer.[27–30] However, auxiliary equipment or multi-step processing is often required. Recently, mussel-inspired chemistry has been widely applied for the preparation of various functional coatings owing to its convenient reaction conditions and universality for virtually any type of surface.[31,32] For example, catechol-functionalized molecules possess excellent binding affinity with diverse material surfaces through coordination or hydrogen bonds.[33,34] In order to construct a surface coating with excellent anti-infective activity for Ti-based implants, we present a new concept combining the antimicrobial biomimetic nanostructure coating and Pep. Better yet, the Pep-functionalized nanostructure coating may also be beneficial for hydroxyapatite (HAp) formation.[35,36] Herein, catechol-ended Pep (cPep) was firstly synthesized by *N*-carboxyanhydride ring-opening polymerization (NCA-ROP) of lysine (Lys) and phenylalanine (Phe) initiated by *tert*-butyldimethylsilyl (TBS)-protected dopamine (Fig. 1A). Secondly, a titania (TiO_2) nanospike coating (TNC) was fabricated on the surface of a Ti substrate through an alkaline hydrothermal process (Fig. 1B). After that, cPep was immobilized onto the TNC surface based on robust coordination bonds between catechol and TiO_2,[37] and the Pep-functionalized TiO_2 nanospike coating (TNPC) was successfully fabricated (Fig. 1C).

2. Materials and methods

2.1. Materials

Medically pure Ti (99.9% purity) was purchased from Xi'an Saite Metal Materials Development Co., Ltd, China. Dopamine hydrochloride, triethyl amine and anhydrous sodium sulfate (Na_2SO_4) were purchased from Sigma-Aldrich and used as received. L-phenylalanine, H-Lys(z)-OH, *tert*-butyldimethylchlorosilane (TMSCl) and triphosgene (98%) were purchased from Tokyo Chemical Industry Co., Ltd. Anhydrous *N*,*N*-dimethylformamide (DMF, 99.8%, superdry, with molecular sieves), trifluoroacetic acid (TFA) and hydrogen bromide (33 wt% solution in acetic acid) were purchased from J&K Scientific Ltd. Anhydrous tetrahydrofuran (THF), diethyl ether, *n*-hexane and dichloromethane (CH_2Cl_2) were obtained using a solvent-drying system from Innovative Technology (PureSolv MD-5). *S. aureus* (ATCC 6538), *E. coli* (ATCC 8739) and *P. aerug*inosa (ATCC 9027) were obtained from the American Type Culture Collection (ATCC). The AlamarBlue™ Cell Viability Assay Reagent and LIVE/DEAD BacLight™ Bacterial Viability Kit were purchased from Thermo Fisher Scientific Inc. Phosphate buffered saline (PBS), Mueller–Hinton (MH) broth and Luria–Bertani (LB) agar, obtained from Sigma-Aldrich, were autoclaved at 121 °C for sterilization before use. High-purity water (Milli-Q) with a resistivity greater than 18 MΩ cm was obtained using an in-line Millipore RiOs/Origin water purification system.

2.2. Characterization

Proton nuclear magnetic resonance (^{1}H-NMR) spectroscopy was conducted using a Varian Unity NMR spectrometer operat-

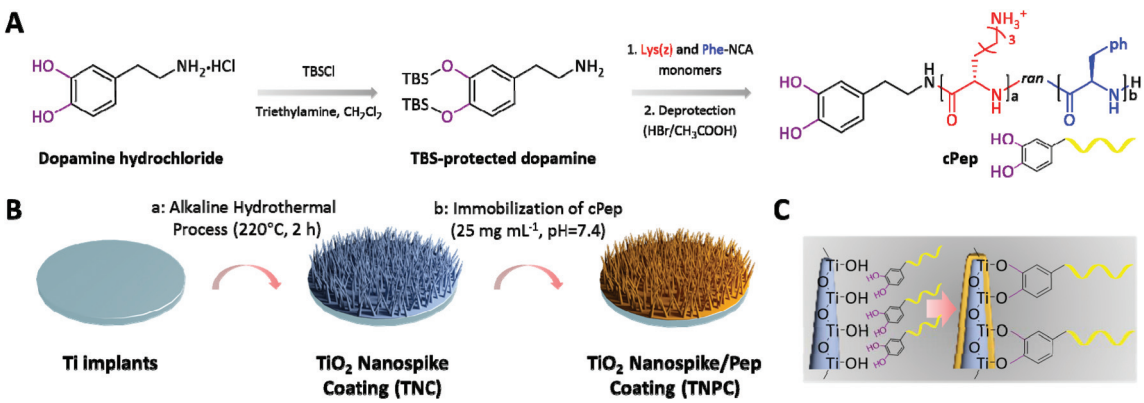

Fig. 1 Illustration of the fabrication process of the TNPC. (A) The synthesis of antibacterial cPep. (B) The preparation of TNPC: (a) fabrication of TNC by an alkaline hydrothermal process; (b) immobilization of cPep onto TNC. (C) Coordinative interactions between catechol groups and TiO_2 nanospikes.

ing at 400 MHz. Chloroform-d ($CDCl_3$), deuterium oxide (D_2O) and deuterated dimethyl sulfoxide (d_6-DMSO) were used as solvents. Fourier-transform infrared spectroscopy (FTIR) was performed on a Bruker Tensor 27 in the mid-infrared range (400–4000 cm^{-1}), and the instrument was equipped with OPUS 6.5 Software and GladiATR with monolithic diamond ATR from Pike Technologies. Typically, 0.1 mg of the coated particle/dried shell sample was ground with dry potassium bromide (KBr) at approximately 1 wt% and the resulting powder was pressed into a transparent pellet using a Specac 10 ton Hydraulic Press. For each sample, 128 scans were taken in transmission mode at a resolution of 2 cm^{-1}. Ultraviolet-visible (UV-vis) absorbance spectra were recorded using a Shimadzu UV-1800 spectrophotometer and UV Probe software package. The wavelength range of 200–700 nm was selected with a medium scan speed and sampling interval of 1 nm. The scan mode was set to be 21 repeats with 3 min interval between scans. X-ray diffraction (XRD) was performed using a Bruker D8 Advance instrument with Cu Kα radiation (λ = 1.5406 Å, 40 kV, 40 mA) and a nickel filter. Diffraction patterns were collected in the 2θ range of 10° to 90° with a step size of 0.04° and 14 s per step. The surface chemical composition was analyzed by X-ray photoelectron spectroscopy (XPS) using an Axis Ultra^{DLD} spectrometer (Kratos Analytical Ltd, UK) with a monochromatic Al-Kα X-ray source (1486.71 eV photons).

2.3. Synthesis of TBS-protected dopamine

The NCA initiator was synthesized based on a previously reported method with suitable modifications.[3] Briefly, dopamine hydrochloride (2 g, 0.01 mol) was added to a flame-dried round-bottom flask, and dissolved in dry CH_2Cl_2 (30 mL) under a nitrogen atmosphere, followed by the addition of TEA (7.33 mL, 0.05 mol) to the reaction mixture. After stirring in an ice/water bath of 0 °C for 5 min, TBSCl (4.77 g, 0.03 mol) in dry CH_2Cl_2 (20 mL) was slowly added at 0 °C. After 2 h, the reaction mixture was removed from the ice/water bath and allowed to warm to room temperature and stirred overnight. The mixture was quenched with HCl solution (1 M, 20 mL) and the organic phase was extracted from the aqueous phase with the use of CH_2Cl_2 (3 × 20 mL). The combined organic layers were then washed with brine (3 × 20 mL), dried over $MgSO_4$, filtered, and concentrated. Purification by flash chromatography (CH_2Cl_2 : CH_3OH = 30 : 1) afforded a yellow solid (1.7 g, 85%). ^{1}H-NMR (400 MHz, $CDCl_3$): δ_H 6.55 (d, 1H, ArH), 6.45 (m, 2H, ArH), 2.93 (t, 2H, $ArCH_2CH_2$), 2.66 (t, 2H, $ArCH_2CH_2$), 1.01 (s, 18H, $-(CH_3)_3$), 0.21 (s, 12H, $-(CH_3)_2-$) ppm.

2.4. Synthesis of cPep

Step (i): Synthesis of TBS-protected dopamine-functionalized polypeptide(z) (TBScPep(z)). Lys(z)-NCA and Phe-NCA were synthesized according to the previously reported method.[29,38] All synthesized NCA monomers were hermetically stored at −80 °C for further use. Lys(z)-NCA (1 g, 3.25 mmol) and Phe-NCA (0.628 g, 3.25 mmol) were transferred into a predried Schlenk-tube equipped with a stir bar under a nitrogen counter flow, followed by drying under high vacuum for 2 h. After the monomers were completely dissolved in dry DMF (20 mL), TBS-protected dopamine (100 mg, 0.26 mmol) was added ($[M_{Lys(z)} + M_{Phe}]/[I_{initiator}]$ = 25). The reaction mixture was stirred at room temperature for 72 h under constant pressure (20 mbar). Then the reaction mixture was precipitated into diethyl ether (50 mL) and was dried under reduced pressure to obtain a white solid. ^{1}H-NMR (400 MHz, d_6-DMSO): δ_H 7.18–7.31 (C_6H_5-), 6.66–6.85 (m, ArH), 4.98 ($-CH_2$), 4.17–4.52 (m, –CH–), 2.76–2.94 (m, $-CH_2-$), 1.1–1.8 (m, $-(CH_2)_3-$), 0.93 ($(-CH_3)_3$), 0.14 ($(-CH_3)_2-$) ppm. *Step ii: Deprotection of TBS-cPep (z)*. TBScPep(z) (200 mg) was dissolved in TFA (5 mL), and HBr in acetic acid (0.5 mL) was slowly added, followed by continuous agitation at 0 °C for 1 h. The deprotected polymer was isolated by the addition of cold ether (40 mL), centrifuged (3200*g*, 5 min), and washed with excess ether (3 × 10 mL). Finally, cPep was dialyzed (MD34, 2000) against deionized water (pH = 5) for 2 days, and subsequently freeze-dried (fluffy white solid, 175 mg, 87.5%). ^{1}H-NMR (400 MHz, D_2O): δ_H 7.29 (C_6H_5-), 6.62–6.83 (m, ArH), 4.08–4.31 (m, –CH–), 2.97 (m, $-CH_2-$), 1.17–1.68 (m, $-(CH_2)_3-$) ppm.

2.5. Fabrication of TNC

Ti disks of 2 mm in thickness were cut from a pure titanium rod (6 mm in diameter) and polished to a mirror shine. All disks were then sonicated in ethanol for 30 min, air-dried, and fully immersed into a custom-made polytetrafluoroethylene (PTEF) hydrothermal synthesis reactor (KH-25 mL) containing NaOH solution (1 M, 5 mL, pH = 13.6). The vessel was tightly sealed and placed in an oven at 220 °C for 2 h. *Caution: When operating at high temperatures, be sure to take protective measures*. Afterwards, the high-temperature steel reaction vessel was quickly put into water, and Ti disks were carefully removed from the holders, rinsed with copious amounts of deionized water, and immersed into HCl solution (0.1 M, 50 mL) for 24 h to exchange sodium ions. Finally, all disks were rinsed with deionized water, and then placed in a furnace for calcination at 550 °C for 3 h.

2.6. Preparation of TNPC

Cleaned TNC was placed in PBS (10 mM, pH = 7.4) containing cPep (25 mg mL^{-1}, 8.94 μM) at room temperature for 24 h. The TNPC was obtained after being washed with large amounts of deionized water and dried in a stream of nitrogen.

2.7. *In vitro* antibacterial assay

The *in vitro* bactericidal potency of the pure Ti, TNC and TNPC disks was determined following a contact protocol.[28] Firstly, all materials were washed with sterile PBS three times and irradiated with UV-light for 30 min. The bacteria (*S. aureus* and *E. coli*) were pre-cultured in MH broth at 37 °C and subcultured until their optical density at 600 nm reached 0.5–0.7. The bacteria were then harvested by centrifugation (1400*g*, 5 min), washed with PBS thrice, and resuspended in PBS at a final concentration of ~10^8 colony forming unit (CFU) mL^{-1}. A 10 μL-aliquot of the inoculum suspension was pipetted and

spread onto the surfaces of pure Ti (control group), TNC and TNPC, then incubated at 37 °C for 1 h. Their antibacterial efficacy was studied by field-emission scanning electron microscopy (FE-SEM) observation and CFU counting. For FE-SEM observation, all samples were fixed with 2.5% glutaraldehyde for 2 h, dehydrated through a series of graded ethanol solutions (20%, 40%, 60%, 80%, 90% and 100%, each for 15 min), lyophilized overnight, and then sputtered with gold for observation. The survived bacteria numbers were determined by CFU counting. Briefly, after a contact time of 1 h, all samples were placed into PBS (1 mL), and vigorously washed and sonicated for 5 min. Then the suspension was plated on agar plates with 10-fold serial dilutions and the CFU was counted, and the antibacterial rate was calculated as: kill% = $[(CFU_{Control} - CFU_{Coating})/CFU_{Control}] \times 100$. All experiments were carried out in triplicate for each formulation.

2.8. LIVE/DEAD baclight bacterial viability assay

Fresh bacterial suspensions of *S. aureus* were grown overnight at 37 °C in MH broth (5 mL). Bacterial cells were collected at the logarithmic stage of growth and the suspensions were adjusted to OD_{600} = 0.01. The pure Ti (control group) and TNPC were individually immersed in the bacterial suspension (2 mL) and incubated at 37 °C for 7 and 14 days to allow biofilm growth. The culture medium was changed every day. Afterwards, all materials were gently washed with sterile PBS to remove unattached planktonic bacteria, stained with the LIVE/DEAD Baclight Bacterial Viability Kit in a dark environment at room temperature for 15 min, and washed with PBS again. Finally, the biofilm formed on the coatings was observed under an inverted fluorescence microscope (IX53, Olympus).

2.9. *In vitro* cytotoxicity

All materials were sterilized with 70% ethanol prior to use. The MC3T3-E1 cell line was obtained from the Cell Bank of the Chinese Academy of Science (Shanghai, China). MC3T3-E1 cells were seeded on a tissue culture polystyrene (TCPS) plate at a density of 6000 cells per cm^2 and cultured for 4 h to allow attachment of the cells. The pure Ti, TNC and TNPC were then individually placed onto the wells, allowing the coatings to contact with the cells. The cells were cultured for 4 days, and the medium was changed every 2 days. The cell viability was determined by AlamarBlue assay at day 1 and 4.[39]

2.10. *In vivo* rodent subcutaneous infection model

For the convenience of animal experiments, Ti rods (Φ = 1 mm, 5 mm in length) were prepared in our laboratory. All animal procedures were performed in accordance with the Guidelines for Care and Use of Laboratory Animals of Xi'an Jiaotong University (Shaanxi, China) and approved by the Animal Ethics Committee of Xi'an Jiaotong University. Male Sprague-Dawley rats (8 weeks, ~200 g) were purchased from the Laboratory Animal Unit of the College of Medicine, Xi'an Jiaotong University, and allowed to acclimatize for 7 days in the lab. For the *in vivo* test, a rat model of implant-associated infection was created by subcutaneously implanting TNPC into the right back of rat, while the left back was implanted with TNC as a control group.[40] The implants were pre-seeded with 10 μL of bacterial suspension (*S. aureus*, 10^8 CFU mL^{-1} in PBS). Post-operatively, all rats were monitored daily. All of the implants were retrieved after 5 days, then individually placed in sterile PBS (1 mL) and sonicated for 5 min to detach the adhered bacteria cells. The bacteria in the resulting suspensions were counted after serial dilutions and plating. In parallel, samples (100 μL) were randomly taken from the resulting bacterial suspensions of each group and placed onto LB agar plates to visualize the bacteria numbers. This procedure was used to verify the absence of bacteria when none was detected by serial dilution plating. For the histological study, the tissues around the implants were sectioned to a thickness of 1–2 mm with sterilized scissors, and immediately fixed in 4% neutral formalin at 4 °C for 4 days for paraffin embedding. The paraffin embedded tissues were cut into 2 mm ultrathin sections. The sections were stained with hematoxylin–eosin colorations and histologically analyzed by light microscopy.

2.11. *In vitro* HAp-forming ability

The SBF was prepared firstly as follows: ultra-pure water (1000 mL) was put into a new plastic beaker and slowly stirred at 36.5 °C, followed by the addition of NaCl, $NaHCO_3$, KCl, $K_2HPO_4{\cdot}3H_2O$, $MgCl_2{\cdot}6H_2O$, $CaCl_2$ and Na_2SO_4 in sequence. *Caution: Ensure that the previous reagent is completely dissolved before adding the next one*. The pH of the solution was found to be approximately 7.5, and tris(hydroxymethyl)aminomethane (Tris)-HCl solution was pipetted to adjust the pH to 7.40 in order to make the pH value and ion concentration similar to those in human plasma. The SBF was stored in a refrigerator at 5–10 °C. The TNPC was separately soaked in SBF (5 mL) at 37 °C for 1, 7 and 14 days, and the SBF was refreshed every 2 days. After that, all samples were gently rinsed with distilled water and lyophilized overnight. The precipitate was imaged by FE-SEM and further measured by energy dispersive spectroscopy (EDX), FTIR and XRD to analyze the elements and components.

Statistical analysis

The results were presented as the mean ± standard deviation. All experimental data were analyzed using Student's *t* test, and $p < 0.05$ was considered to be statistically significant.

3. Results and discussion

3.1. Functionalization of cPep onto TNC

Contact-active antibacterial surfaces are usually fabricated with the immobilization/grafting of molecules such as bactericides, cationic polymers and antimicrobial peptides.[41] The excellent antibacterial activity in solution, is one of the key factors for the selection of these molecules.[42,43] In this work, we chose a cationic polypeptide (cPep) which has potent broad-spectrum antibacterial activity in solution, to construct a contact-active antibacterial surface on a nanostructured Ti surface.[44] cPep

was synthesized through NCA-ROP initiated by TBS-protected dopamine firstly. The phenolic hydroxyl groups of dopamine were protected in advance so as to ensure that only the amine group is used for the initiation of NCA monomers. Following our previously optimized composition, antibacterial cPep was synthesized by the copolymerization of carboxybenzyl (Cbz)-protected-Lys (cationic segment) and Phe (hydrophobic segment) at the molar ratio of 1 : 1, with a total chain length of 25 amino acids. Thereafter, the TBS and Cbz protecting groups were removed in one step under acidic conditions. The ^{1}H-NMR spectra of cPep showed the characteristic chemical shifts of catechol groups at 6.62, 6.78 and 6.83 ppm, while the corresponding signals for Cbz and TBS protecting groups disappeared after the deprotection process (Fig. S1†). Furthermore, the UV-vis absorption spectra of the cPep polymer indicated the characteristic absorption peak of catechol groups at 280 nm,[45] confirming the successful introduction of dopamine (Fig. S2†). By quantitatively measuring the catechol groups in cPep according to the standard curve of dopamine, the molecular weight of cPep was determined to be 2796.2 g mol^{-1}. It is worth mentioning that the presence of catechol groups did not affect its antibacterial efficacy. cPep exhibited an excellent minimum inhibitory concentration (MIC) of 31 μg mL^{-1} (11.1 μM) against three clinically significant pathogens, including Gram-positive (*S. aureus*) and Gram-negative (*E. coli* and *P. aeruginosa*) bacteria, which is the same as Pep (Table S1†).

TNC was fabricated *via* an alkali hydrothermal process followed by annealing treatment. As shown in Fig. 2A, spike-like nanofibers with an average diameter of 47 ± 5 nm were generated after alkali-heat treatment at 220 °C for 2 h in 1 M NaOH solution, followed by annealing treatment at 550 °C for 3 h. A layer of nanofibers with a thickness of about 4 μm homogenously covered on the Ti surface (Fig. 2B). The chemical composition of the coating was analyzed by XRD and EDX. As shown in Fig. 2C and D, the TNC was mainly comprised of TiO_2. Thus the O content was significantly increased in TNC as compared with the pure Ti, owing to the formation of large amounts of Ti-OH groups. A nanostructured coating provides two additional advantages for implant applications, including expanding the surface area and improving the mechanical locking force to increase the primary stability of the implant, as well as enhancing implant anchorage by allowing bone ingrowth.[46,47] In addition, the morphology of the TNC layer did not change after ultrasound treatment for 30 min, indicating its good stability on the surface (Fig. S3†).

TNPC was fabricated through the functionalization of cPep onto the TNC surface and characterized by FTIR, contact angle measurement and XPS to verify the successful preparation (Fig. 3). In the FTIR spectra, TNPC exhibited characteristic vibration peaks for cPep, which were at 3000–3400, 2900, 1640 and 1530 cm^{-1} for –NH_x/–OH and –CH_2– stretching vibrations as well as amide I and II bands, respectively (Fig. 3A).[27] As shown in Fig. 3B, pure Ti indicated a less hydrophilic character with a contact angle of 66 ± 1°, while its wettability was markedly improved after surface treatment, with contact angles of 8 ± 1° and 12 ± 2° for TNC and TNPC, respectively. Moreover, TNPC showed a new peak at 399.3 eV for N1s in the XPS

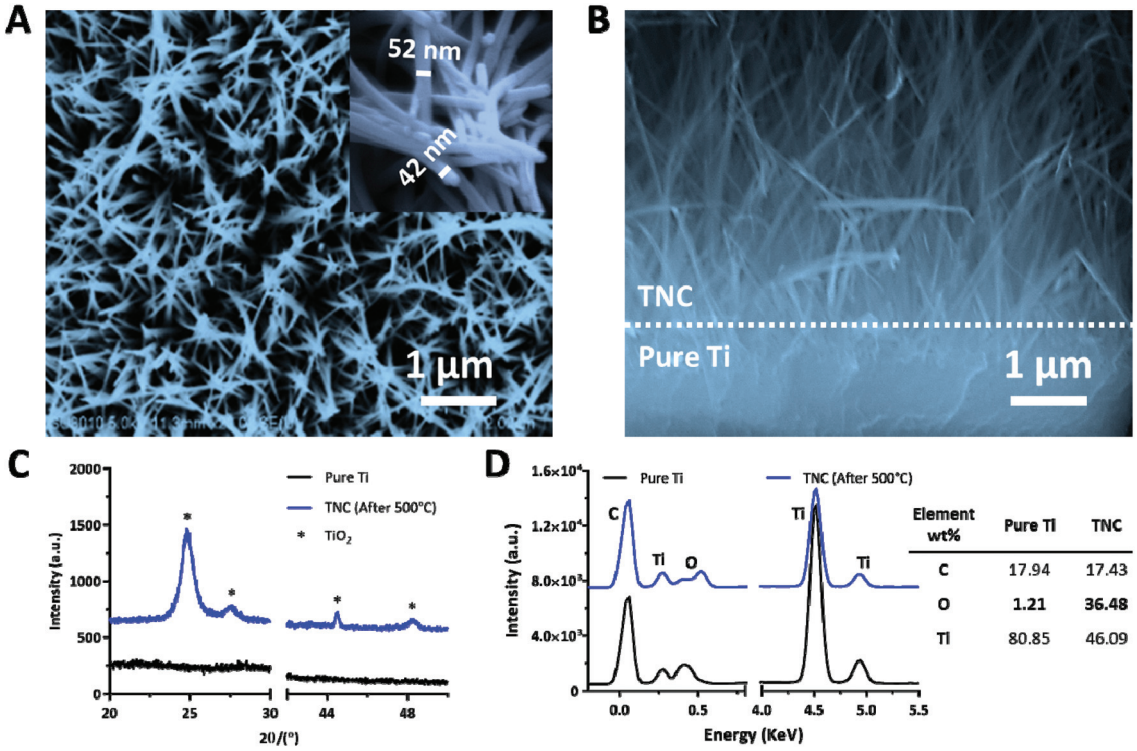

Fig. 2 (A) FE-SEM and (B) cross section of the TNC. (C) XRD and (D) EDX of the pure Ti and TNC.

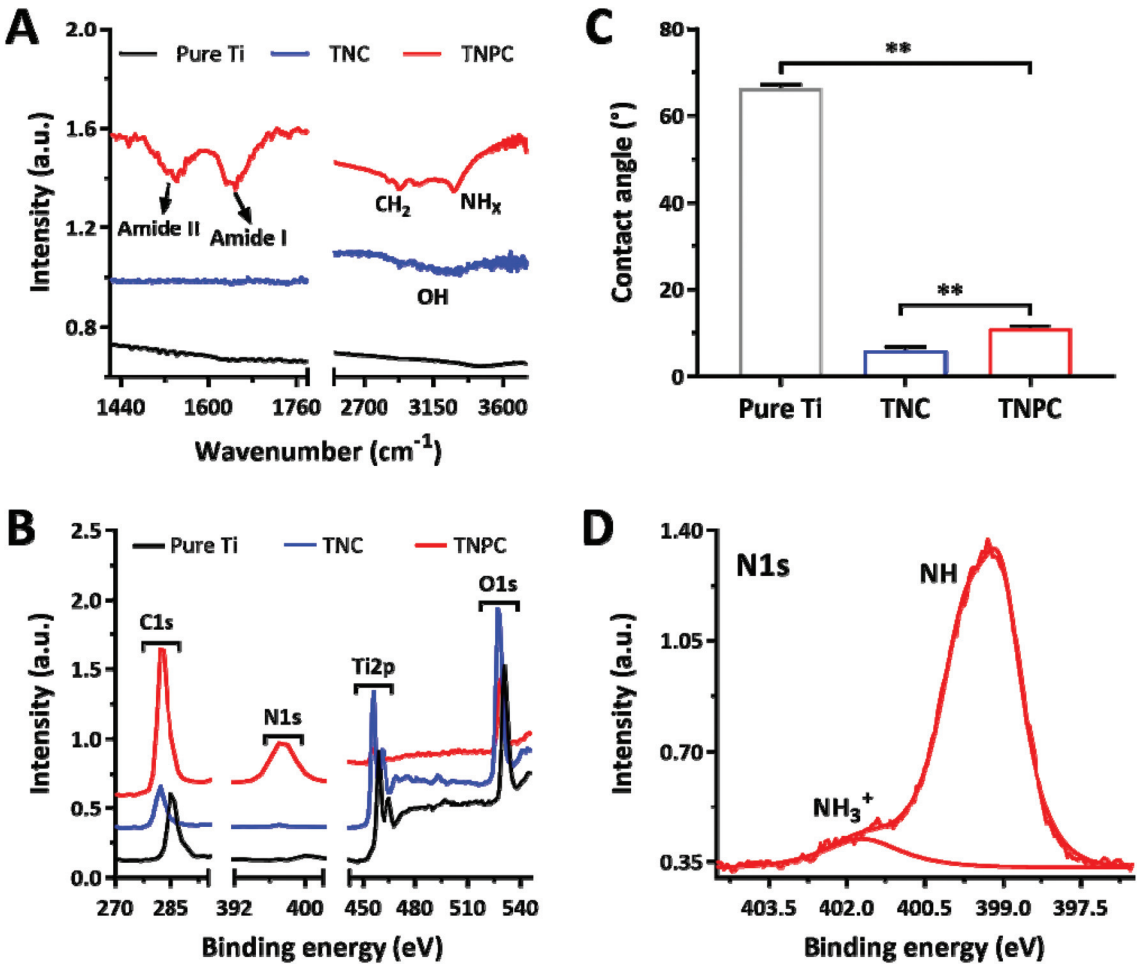

Fig. 3 (A) FTIR spectra, (B) contact angle and (C) XPS spectra of the pure Ti, TNC and TNPC. (D) High-resolution (N1s) XPS spectra of the TNPC.

spectra (Fig. 3C), which was attributed to the –NH– (399.2 eV) and $-NH_3^+$ (401.8 eV) existing in the cPep (Fig. 3D),[27] and these results revealed the successful immobilization of cPep onto TNC.

3.2. *In vitro* antibacterial studies

The bactericidal efficiency of the TNC and TNPC was evaluated against two kinds of pathogenic bacteria (*S. aureus* and *E. coli*) through a surface contact protocol with pristine Ti as the control group.[29,48] Firstly, FE-SEM was used to visualize the bacterial morphology on different surfaces after 1 h culture. As shown in Fig. 4A, both *S. aureus* and *E. coli* were observed on the pristine Ti surface with significant quantity and intact morphology. When bacteria were incubated on the surface of TNC, bacteria were located on or between the nanospikes. Notably, although some of the bacteria still kept their normal shape, morphological deformation was observed (blue arrows). In marked contrast, the TNPC surface disrupted *S. aureus* and *E. coli* cells more effectively, and most of the contacted bacteria had significant morphology changes. It was clearly revealed that both *S. aureus* and *E. coli* cells collapsed and deformed (red arrows). These results indicate that TNC could disrupt the contacted bacteria partially, which coincides with previous studies.[49] Whereas with the immobilization of cPep, TNPC exhibits a stronger effect of disturbance and destroys bacterial cells. To further verify this phenomenon and investigate their viability, the bacteria after contact with the surfaces were collected and re-cultured for CFU counting.

S. aureus and *E. coli* were inoculated on the surface of pure Ti, TNC and TNPC at a concentration of ~10^8 CFU mL^{-1}. Upon incubation for 1 h, the colony numbers of each type of bacteria were significantly reduced for TNC and TNPC (Fig. 4B). 52.2% of *S. aureus* and 72.9% of *E. coli* were dead on contact with TNC, which indicated the significant ($p < 0.01$) disruption of the bacteria by TiO_2 nanospikes. It seemed that TNC is more potent to kill Gram-negative *E. coli* than Gram-positive *S. aureus*. By contrast, TNPC showed a greatly enhanced killing efficiency of more than 99.9% toward both *S. aureus* and *E. coli*.

Previous studies had demonstrated that such nanospike surfaces possess antibacterial activity owing to their high aspect ratio nanostructure induced extensional deformation of the attached bacteria.[17,49] Gram-positive bacteria have thick peptidoglycan multilayers outside the cytoplasmic membrane (*e.g.*, 20 layers for *S. aureus* with a thickness of ~20 nm), which

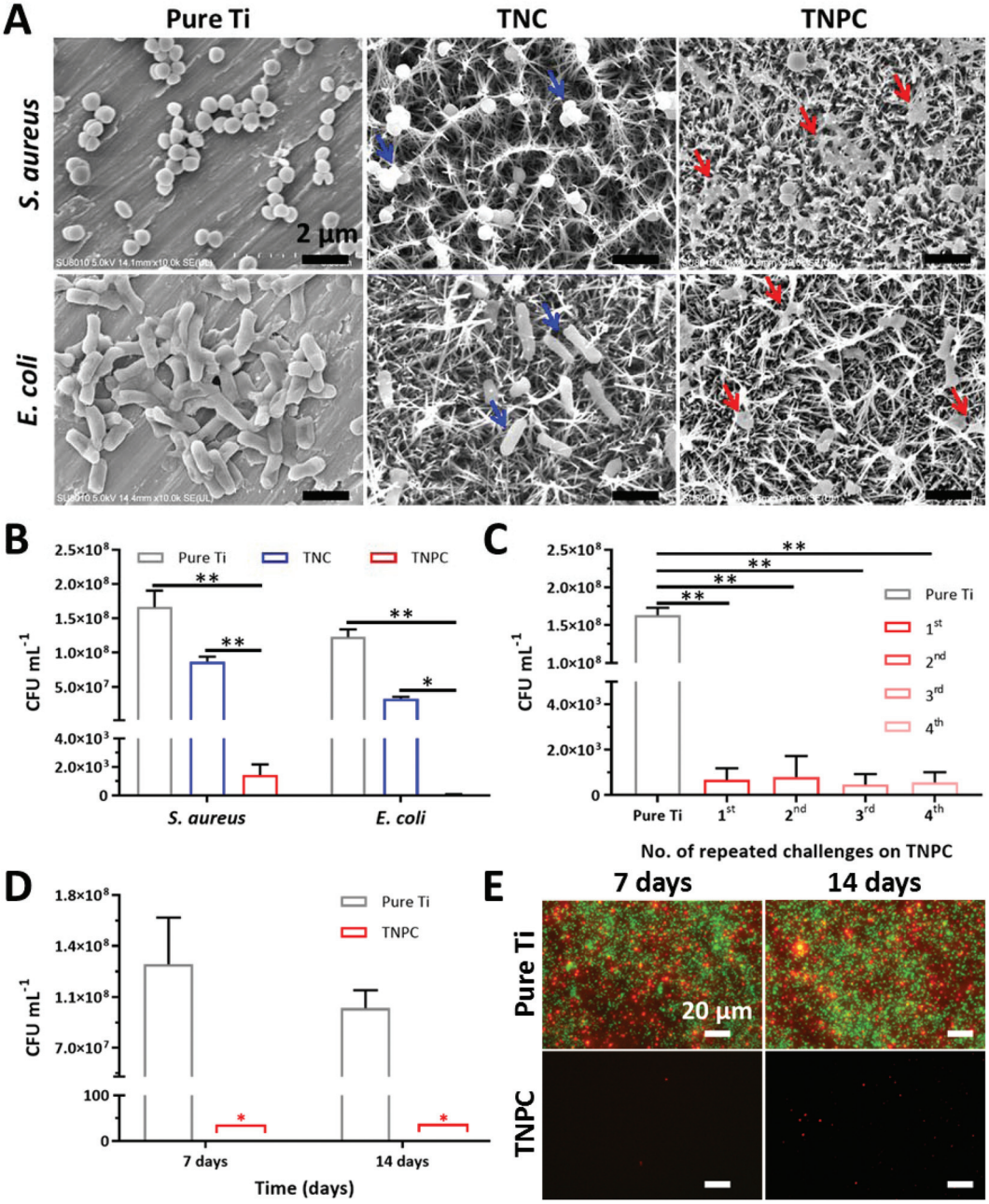

Fig. 4 (A) FE-SEM of bacterial cells after 1 h incubation on the surfaces of flat pure Ti, TNC and TNPC, blue and red arrows point to exemplar piercing sites. (B) Antibacterial activity of the flat pure Ti (control group), TNC and TNPC surfaces. (C) Long-term antibacterial activity of the TNPC surfaces against *S. aureus*. (D) CFU numbers and (E) LIVE/DEAD bacterial viability assay of *S. aureus* after being in contact with the pure Ti (control group) and TNPC for 7 and 14 days. (Each data point represents the mean ± standard deviation, n = 3).

cross-linked into a tight network thus forming a more rigid cell wall.[50] In contrast, Gram-negative bacteria only have a thin peptidoglycan layer (*e.g.*, 3 layers for *E. coli* with a thickness of ~3 nm) and an outer lipid membrane with fluidity. Therefore, *S. aureus* cells are less susceptible to the nanospike structure of TNC. When bacteria were in contact with the nanospike structure, the bacterial cell was stretched on the surface, leading to membrane rupture, and bacteria death. However, the bacteria could not be completely killed only by this physical-mechanical effect. With the modification of cationic antibacterial Pep on the nanospike, both *S. aureus* and *E. coli* cells were strongly disrupted by TNPC with an excellent kill ratio of above 99.9%. What is more, the cell wall and membrane of bacteria are composed of anionic molecules (*e.g.*, lipopolysaccharides for Gram-negative bacteria, teichoic acids for Gram-positive bacteria). The surface tethered cations could strengthen the interaction of nanospikes with anionic bacterial cells, thus leading to exceptional bactericidal efficacy.

3.3. Long-term antibacterial and antibiofilm efficacies

After implantation, orthopedic implants usually need a period of time for the integration with the surrounding tissue.[4] Before the successful osseointegration of implants, their interface could be an ideal seedbed for bacteria. Thus, patients carry the risk of infection in the first few weeks after implantation due to the continuous challenge of opportunistic pathogens.[9,51] Hence, an antibacterial coating that could resist multiple attacks of bacteria and maintain its long-time efficacy is desirable. To ascertain its durable antibacterial efficacy, our TNPC was repeatedly challenged with *S. aureus* four times. As shown in Fig. 4C, the TNPC still possessed excellent antibacterial efficacy above 99.9% even after the forth challenge with bacteria of high concentrations ($\sim 10^8$ CFU mL^{-1}).

Once bacteria managed to adhere on the surface of implants, it could develop into a biofilm shortly. Bacteria in the biofilm are hard to kill as the bacteria are embedded in a protective polymeric matrix.[52,53] Accordingly, biofilm-associated implant infections are hard to treat. Although the biofilm-infected implants could be removed by surgery, the residual biofilm hiding in the body still can cause recurring infections.[5,54] Thus, biofilm-resistance is a key factor for antibacterial coatings of implants. Herein, the antibiofilm activity of TNPC was studied with *S. aureus* for 7 and 14 days. As proved by the number of CFUs, abundant bacteria could adhere on the surface of pure Ti at day 7 and 14, while almost no adherent bacteria could be detected on the surface of TNPC (Fig. 4D). Moreover, the LIVE/DEAD bacterial viability assay showed that the *S. aureus* biofilm with copious alive bacterial cells (stained green) were formed upon the pure Ti surface, but only few dead bacteria (stained red) could be observed on TNPC at day 7 and 14 (Fig. 4E). These results demonstrated that our TNPC has durable antibacterial and antibiofilm properties.

3.4. *In vitro* cytotoxicity assay

With the development of medical science and technology, more and more orthopedic implants are widely used in clinical practice. However, although they have achieved satisfactory results in orthopedic treatment, and since orthopedic implants are inevitably in contact with human tissues, blood and cells, their cytotoxicity is a primary criterion for clinical applications. The *in vitro* cytotoxicity of the pure Ti, TNC and TNPC was evaluated by the AlamarBlue assay, and they were respectively cultured with murine MC3T3-E1 osteoblastic cells for 4 days. An unmodified TCPS plate was used as the control. At day 1 and 4, the cell viability was determined by the AlamarBlue staining. As shown in Fig. 5, murine osteoblastic cells could keep growing for up to 4 days when in contact with the pure Ti, TNC and TNCP surfaces. It turned out that there was no significant difference ($p > 0.05$) in the viability of osteoblastic cells cultured on TCPS, pure Ti, TNC and TNPC. This result identified that the pure Ti, TNC and TNPC were non-toxic to the growth of osteoblastic cells.

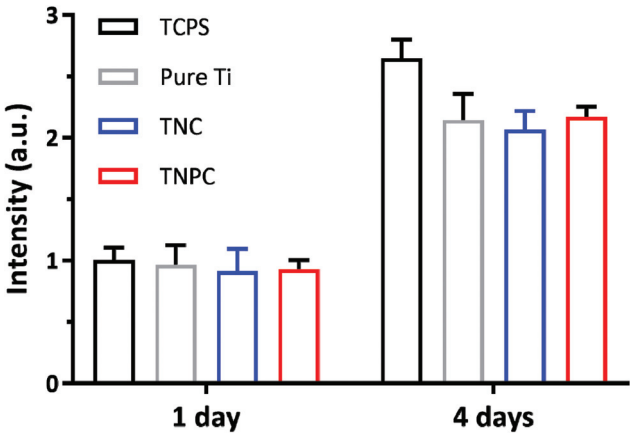

Fig. 5 *In vitro* cytotoxicity study of the pure Ti, TNC and TNPC with murine MC3T3-E1 osteoblastic cells determined by AlamarBlue assay at 1 and 4 days (error bars represent mean ± standard deviation for $n = 5$). MC3T3-E1 cell growth was unaffected by incubation with the pure Ti, TNC and TNPC for up to 4 days. No significant difference ($p > 0.05$) in the viability of osteoblastic cells in contact with the TCPS (control group), pure Ti, TNC and TNPC.

3.5. *In vivo* anti-infective activity

To further evaluate the *in vivo* anti-infective ability of TNPC, a rat subcutaneous infection model was constructed with *S. aureus* bacteria, one of the key pathogenic microbes resulting in medical implant-associated infections.[55] The infection was induced through a pre-seeding protocol.[56] Incisions (~1 cm) were cut on two sides of each rat's back, and the pure Ti (left) and TNPC (right) modified Ti rods pre-contaminated with fresh *S. aureus* of $\sim 10^6$ CFU were then placed into the incisions on a total of 8 rats (Fig. 6A). After 5 days, the infection condition at the implantation site was observed. As shown in Fig. 6B, severe bacterial infection was clearly observed around the pure Ti implant. In contrast, the tissue was normal around the TNPC implant, with no obvious infection observed. The TNPC implant had better wound healing performance due to its available antibacterial activity.[26] All implants were retrieved and washed with sterilized PBS under ultrasonication, followed by determining the number of viable bacteria on the implants. As shown in Fig. 6C, there were numerous *S. aureus* bacteria growing on the pure Ti implants ($\sim 3.26 \times 10^8$ CFU), but few bacteria were retrieved from the TNPC implants (~28 CFU). Moreover, all eight pure Ti implants were seriously infected with the bacteria number ranging from 4.90×10^7 to 5.73×10^8 CFU per implant, whereas one of the eight TNPC implants had no visible bacteria and the other seven had fewer than 450 CFU per implant (Fig. 6D). The number of adherent bacteria on the TNPC implants was significantly lower than those on the pure Ti implants, with a log reduction of 6.65 ($p < 0.001$). In addition, histological analysis was further used to evaluate the anti-infective effect of the TNPC implants by hematoxylin–eosin (H&E) staining. As shown in Fig. 6E, more inflammatory neutrophils (stained blue) were

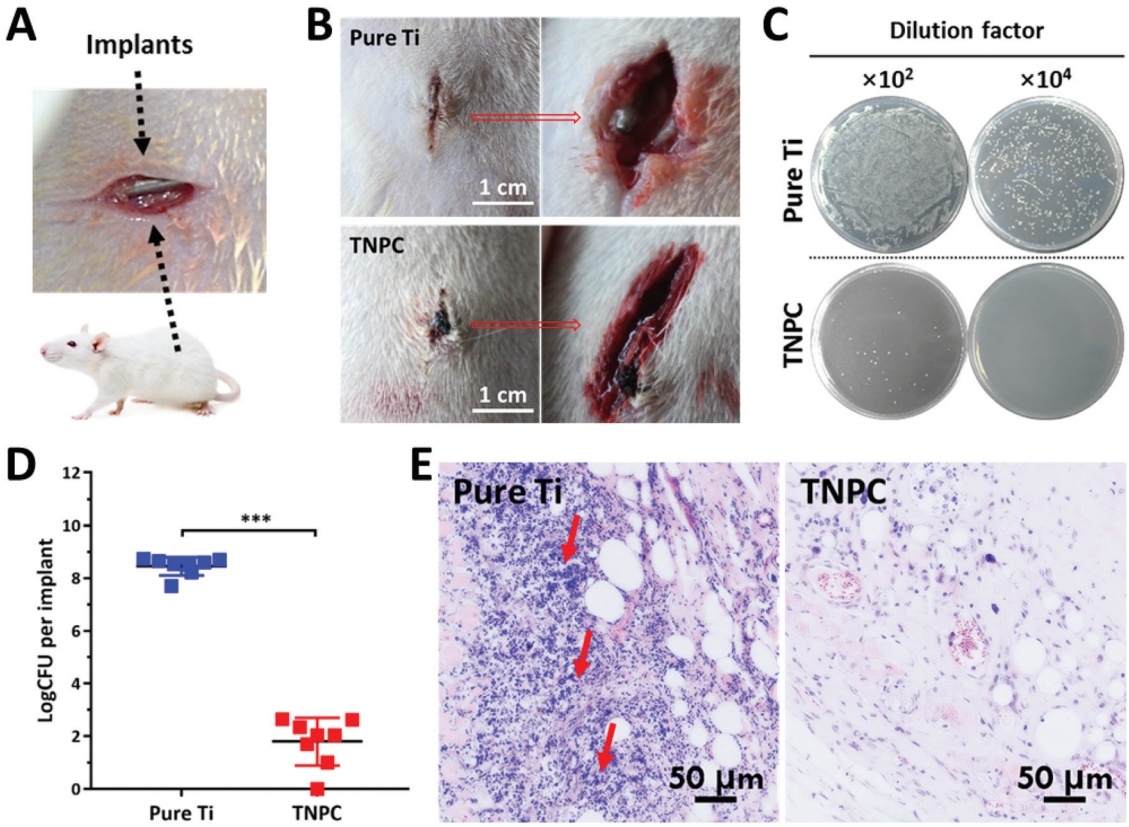

Fig. 6 *In vivo* anti-infective activity of the pure Ti and TNPC. (A) Scheme of the rat subcutaneous infection model. (B) Photographs of a rat implanted with both the pure Ti and TNPC on day 5. The inflammation at the wound site in two groups was visually observed. (C) Photographs of the spread plate of the pure Ti and TNPC implants (10^2 and 10^4 mean degree of dilution). (D) Numbers of viable *S. aureus* recovered from the pure Ti and TNPC implant surface after 5 days in the subcutaneous rat model ($p < 0.001$). The black lines represent the average value of each group. (E) Histological study of the infected tissues around the pure Ti and TNPC implants (the red arrows indicate the inflammatory area).

observed in the tissue around the pure Ti implants in comparison with those around the TNPC implants. These results indicated that the TNPC implants had excellent *in vivo* anti-infective activity.

3.6. Biomimetic HAp formation

The ability to induce the surficial growth of HAp in a physiological environment is an important factor to evaluate the bioactivity or bone conductivity of the orthopedic implants.[35] It is known that HAp formation is effectively enhanced by functional groups (*e.g.*, carboxyl, hydroxyl and amine groups),[57–59] and the TNPC contains enriched groups of the positively charged amine, which are able to absorb the negatively charged phosphates and carbonates by electrostatic interactions.[60] The absorbed phosphates and carbonates are able to attract the calcium ions, thus leading to the eventual deposition of HAp with carbonates. After soaking for 7 and 14 days, a newly precipitated layer covered on the TNPC surface, as proved by FE-SEM results (Fig. 7A). FTIR and XRD were then applied to characterize the structure of the HAp grown on the TNPC surface at day 7 and 14, respectively. As shown in Fig. 7B, the vibration peaks at 1035, 600 and 575 cm^{-1} were ascribed to the stretching and bending vibrations of PO_4^{3-}, revealing the successful formation of crystalline HAp. Moreover, the vibration bands at 1545, 1450 and 875 cm^{-1} were attributed to the stretching and bending vibrations of CO_3^{2-}, indicating that trace amounts of PO_4^{3-} were substituted by CO_3^{2-} to form A-type of carbonated HAp,[61,62] which possessed improved solubility and degradability for the replacement of new bones and osseointegration. In addition, –OH and H_2O molecules were also observed in the precipitated layer due to the presence of the corresponding vibration peaks at 3450, 1655 and 645 cm^{-1}.[59] XRD analysis proved that the mineral grown on the TNPC surface was HAp. As shown in Fig. 7C, the HAp phase can be determined through the XRD peaks at 25.8°, 28.5°, 34.8° and 49.5° for the reflection planes of (002), (210), (211) and (213), respectively.[35,63] Furthermore, large amounts of O, P and Ca, as well as tiny amounts of Na and Ti were detected by EDX (Fig. 7D). According to the EDX results the Ca/P ratio of the deposited coatings (1.62) was close to that of stoichiometric HAp (Ca/P = 1.67). These results indicated that the TNPC possessed excellent bioactivity for the *in situ* formation of HAp.

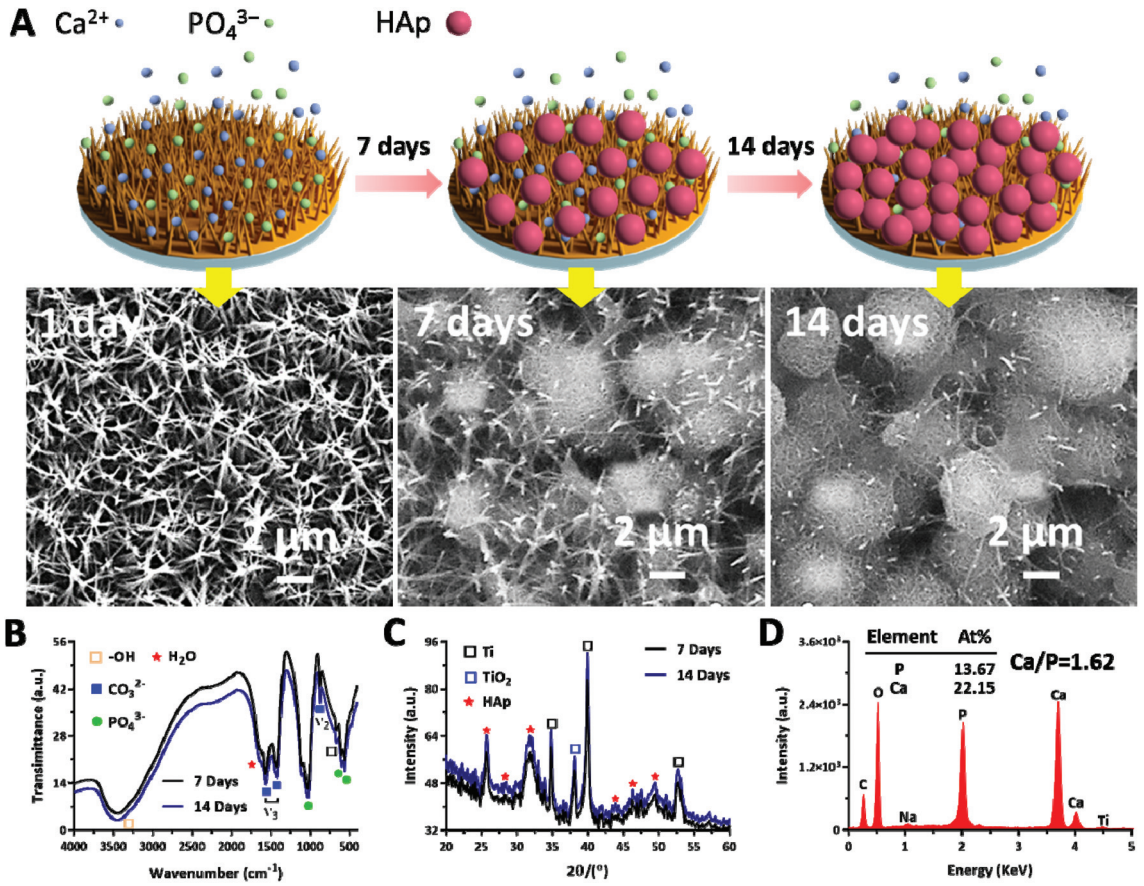

Fig. 7 (A) Process for the accumulation of calcium phosphate biominerals on the TNPC surface and FE-SEM images of the HAp growth at day 1, 7 and 14. (B) The chemical structure of the HAp on the TNPC at 7 and 14 days verified by FTIR, respectively. (C) The XRD pattern of the HAp on the TNPC at day 7 and 14, respectively. (D) Results of EDX elemental analysis inside the HAp crystals on day 14.

4. Conclusion

In this work, the rationally designed bactericidal cPep possessing catechol groups was first directly synthesized by a one-step NCA-ROP, with the purpose that this mussel-inspired Pep could be easily immobilized onto the nanospike TNC surface through robust coordinative interaction between catechol and TiO_2. TNPC showed enhanced antibacterial activity with an inhibition rate of more than 99.9% against both Gram-positive and Gram-negative bacteria. Moreover, inferring from the *in vivo* rat infection model results, TNPC displayed strong anti-infective properties, while reserving excellent biocompatibility with non-toxicity to murine osteoblastic cells, and the number of bacteria in the infected implant has even been reduced by 6 orders of magnitude. Simultaneously, TNPC could induce the deposition of HAp from SBF, indicating that it could potentially promote the bioactivity of the Ti-based implants. Overall, due to the flexibility in design and fabrication, this dual-functional novel coating with antibacterial and biological activity holds great promise for utilization with orthopedic and dental implants.

Conflicts of interest

There are no conflicts to declare.

Acknowledgements

This work was financially supported by the National Key R&D Program of China (2018YFC1105402 and 2017YFA0207202), the National Natural Science Foundation of China (21875189), the Key R&D Program of Jiangsu Province (BE201740), the Innovative Talents Promotion Project of Shaanxi Province (2019KJXX-064 and 2019JQ-157), and the Fundamental Research Funds for the Central Universities.

References

1 M. Geetha, A. K. Singh, R. Asokamani and A. K. Gogia, *Prog. Mater. Sci.*, 2009, **54**, 397–425.
2 A. M. Khorasani, M. Goldberg, E. H. Doeven and G. Littlefair, *J. Biomater. Tissue Eng.*, 2015, **5**, 593–619.

3 N. Jiang, Z. J. Guo, D. Sun, Y. B. Li, Y. T. Yang, C. Chen, L. Zhang and S. S. Zhu, *ACS Nano*, 2018, **12**, 7883–7891.
4 G. Q. Pan, S. J. Sun, W. Zhang, R. B. Zhao, W. G. Cui, F. He, L. X. Huang, S. H. Lee, K. J. Shea, Q. Shi and H. L. Yang, *J. Am. Chem. Soc.*, 2016, **138**, 15078–15086.
5 C. R. Arciola, D. Campoccia and L. Montanaro, *Nat. Rev. Microbiol.*, 2018, **16**, 397–409.
6 S. Renvert and M. Quirynen, *Clin. Oral Implants Res.*, 2015, **26**, 15–44.
7 S. Spriano, S. Yamaguchi, F. Baino and S. Ferraris, *Acta Biomater.*, 2018, **79**, 1–22.
8 P. Liu, Y. S. Hao, Y. C. Zhao, Z. Yuan, Y. Ding and K. Y. Cai, *Colloids Surf., B*, 2017, **160**, 110–116.
9 J. Li, L. Tan, X. M. Liu, Z. D. Cui, X. J. Yang, K. W. K. Yeung, P. K. Chu and S. L. Wu, *ACS Nano*, 2017, **11**, 11250–11263.
10 E. P. Ivanova, J. Hasan, H. K. Webb, V. K. Truong, G. S. Watson, J. A. Watson, V. A. Baulin, S. Pogodin, J. Y. Wang, M. J. Tobin, C. Lobbe and R. J. Crawford, *Small*, 2012, **8**, 2489–2494.
11 D. E. Mainwaring, S. H. Nguyen, H. Webb, T. Jakubov, M. Tobin, R. N. Lam, A. H. F. Wu, R. Marchant, R. J. Crawforda and E. P. Ivanova, *Nanoscale*, 2016, **8**, 6527–6534.
12 V. Felipe, N. B. Iván, J. H. Jaime, R. O. Manuel and R. Isabel, *Bioinspiration Biomimetics*, 2018, **13**, 026011.
13 G. S. Watson, D. W. Green, L. Schwarzkopf, X. Li, B. W. Cribb, S. Myhra and J. A. Watson, *Acta Biomater.*, 2015, **21**, 109–122.
14 A. Tripathy, P. Sen, B. Su and W. H. Briscoe, *Adv. Colloid Interface Sci.*, 2017, **248**, 85–104.
15 A. Jaggessar, H. Shahali, A. Mathew and P. Yarlagadda, *J. Nanobiotechnol.*, 2017, **15**, 64.
16 A. Elbourne, R. J. Crawford and E. P. Ivanova, *J. Colloid Interface Sci.*, 2017, **508**, 603–616.
17 E. P. Ivanova, J. Hasan, H. K. Webb, G. Gervinskas, S. Juodkazis, V. K. Truong, A. H. Wu, R. N. Lamb, V. A. Baulin, G. S. Watson, J. A. Watson, D. E. Mainwaring and R. J. Crawford, *Nat. Commun.*, 2013, **4**, 2838.
18 G. Hazell, L. E. Fisher, W. A. Murray, A. H. Nobbs and B. Su, *J. Colloid Interface Sci.*, 2018, **528**, 389–399.
19 L. E. Fisher, Y. Yang, M. F. Yuen, W. J. Zhang, A. H. Nobbs and B. Su, *Biointerphases*, 2016, **11**, 011014.
20 F. Viela, I. Navarro-Baena, A. Jacobo-Martín, J. J. Hernández, M. Boyano-Escalera, M. R. Osorio and I. Rodríguez, *RSC Adv.*, 2018, **8**, 22606–22616.
21 M. Yamada, K. Minoura, T. Mizoguchi, K. Nakamatsu, T. Taguchi, T. Kameda, M. Sekiguchi, T. Suzutani and S. Konno, *PLoS One*, 2018, **13**, e0198300.
22 E. P. Ivanova, S. H. Nguyen, Y. C. Guo, V. A. Baulin, H. K. Webb, V. K. Truong, J. V. Wandiyanto, C. J. Garvey, P. J. Mahon, D. E. Mainwaring and R. J. Crawford, *Acta Biomater.*, 2017, **59**, 148–157.
23 D. L. Gonzalez Arellano, K. W. Kolewe, V. K. Champagne, I. S. Kurtz, E. K. Burnett, J. A. Zakashansky, F. D. Arisoy, A. L. Briseno and J. D. Schiffman, *Sci. Rep.*, 2018, **8**, 11618.
24 J. P. Penaloza, V. Marquez-Miranda, M. Cabana-Brunod, R. Reyes-Ramirez, F. M. Llancalahuen, C. Vilos, F. Maldonado-Biermann, L. A. Velasquez, J. A. Fuentes, F. D. Gonzalez-Nilo, M. Rodriguez-Diaz and C. Otero, *J. Nanobiotechnol.*, 2017, **15**, 1.
25 J. Hasan, H. K. Webb, V. K. Truong, S. Pogodin, V. A. Baulin, G. S. Watson, J. A. Watson, R. J. Crawford and E. P. Ivanova, *Appl. Microbiol. Biotechnol.*, 2013, **97**, 9257–9262.
26 J. Ye, J. J. Deng, Y. T. Chen, T. Yang, Y. L. Zhu, C. X. Wu, T. L. Wu, J. Y. Jia, X. G. Cheng and X. L. Wang, *Biomater. Sci.*, 2019, **7**, 2826–2832.
27 Q. Gao, P. Li, H. Y. Zhao, Y. S. Chen, L. Jiang and P. X. Ma, *Polym. Chem.*, 2017, **8**, 6386–6397.
28 Y. J. Su, Z. L. Zhi, Q. Gao, M. H. Xie, M. Yu, B. Lei, P. Li and P. X. Ma, *Adv. Healthcare Mater.*, 2017, **6**, 1601173.
29 Q. Gao, M. Yu, Y. J. Su, M. H. Xie, X. Zhao, P. Li and P. X. Ma, *Acta Biomater.*, 2017, **51**, 112–124.
30 Z. L. Zhi, Y. J. Su, Y. W. Xi, L. Tian, M. Xu, Q. Q. Wang, S. Padidan, P. Li and W. Huang, *ACS Appl. Mater. Interfaces*, 2017, **9**, 10383–10397.
31 J. H. Ryu, P. B. Messersmith and H. Lee, *ACS Appl. Mater. Interfaces*, 2018, **10**, 7523–7540.
32 T. G. Barclay, H. M. Hegab, S. R. Clarke and M. Ginic-Markovic, *Adv. Mater. Interfaces*, 2017, **4**, 1601192.
33 J. Y. Park, J. Yeom, J. S. Kim, M. Lee, H. Lee and Y. S. Nam, *Macromol. Biosci.*, 2013, **13**, 1511–1519.
34 J. Saiz-Poseu, J. Mancebo-Aracil, F. Nador, F. Busque and D. Ruiz-Molina, *Angew. Chem., Int. Ed.*, 2019, **58**, 696–714.
35 Y. Ha, J. Yang, F. Tao, Q. Wu, Y. J. Song, H. R. Wang, X. Zhang and P. Yang, *Adv. Funct. Mater.*, 2018, **28**, 1704476.
36 M. Sarem, S. Ludeke, R. Thomann, P. Salavei, Z. Zou, W. Habraken, A. Masic and V. P. Shastri, *Adv. Mater.*, 2017, **29**, 1701629.
37 M. Pagel, R. Hassert, T. John, K. Braun, M. Wiessler, B. Abel and A. G. Beck-Sickinger, *Angew. Chem., Int. Ed.*, 2016, **55**, 4826–4830.
38 P. Li, C. C. Zhou, S. Rayatpisheh, K. Ye, Y. F. Poon, P. T. Hammond, H. W. Duan and M. B. Chan-Park, *Adv. Mater.*, 2012, **24**, 4130–4137.
39 Y. J. Su, L. Tian, M. Yu, Q. Gao, D. H. Wang, Y. W. Xi, P. Yang, B. Lei, P. X. Ma and P. Li, *Polym. Chem.*, 2017, **8**, 3788–3800.
40 J. Gu, Y. J. Su, P. Liu, P. Li and P. Yang, *ACS Appl. Mater. Interfaces*, 2017, **9**, 198–210.
41 Z. K. Zander and M. L. Becker, *ACS Macro Lett.*, 2017, **7**, 16–25.
42 Y. X. Qian, F. Qi, Q. Chen, Q. Zhang, Z. Q. Qiao, S. Zhang, T. Wei, Q. Yu, S. Yu, Z. W. Mao, C. Y. Gao, Y. R. Ding, Y. Y. Cheng, C. Y. Jin, H. X. Xie and R. H. Liu, *ACS Appl. Mater. Interfaces*, 2018, **10**, 15395–15400.
43 C. Yang, X. Ding, R. J. Ono, H. Lee, L. Y. Hsu, Y. W. Tong, J. Hedrick and Y. Y. Yang, *Adv. Mater.*, 2014, **26**, 7346–7351.
44 C. C. Zhou, X. B. Qi, P. Li, W. N. Chen, L. Mouad, M. W. Chang, S. S. J. Leong and M. B. Chan-Park, *Biomacromolecules*, 2010, **11**, 60–67.

45 S. Hong, K. Yang, B. Kang, C. Lee, I. T. Song, E. Byun, K. I. Park, S. W. Cho and H. Lee, *Adv. Funct. Mater.*, 2013, **23**, 1774–1780.
46 Y. Zhukova and E. V. Skorb, *Adv. Healthcare Mater.*, 2017, **6**, 1600914.
47 R. Rasouli, A. Barhoum and H. Uludag, *Biomater. Sci.*, 2018, **6**, 1312–1338.
48 P. Li, Y. F. Poon, W. F. Li, H. Y. Zhu, S. H. Yeap, Y. Cao, X. B. Qi, C. C. Zhou, M. Lamrani, R. W. Beuerman, E. T. Kang, Y. G. Mu, C. M. Li, M. W. Chang, S. S. Leong and M. B. Chan-Park, *Nat. Mater.*, 2011, **10**, 149–156.
49 T. Diu, N. Faruqui, T. Sjostrom, B. Lamarre, H. F. Jenkinson, B. Su and M. G. Ryadnov, *Sci. Rep.*, 2014, **4**, 7122.
50 S. J. Kim, J. Chang and M. Singh, *Biochim. Biophys. Acta, Biomembr.*, 2015, **1848**, 350–362.
51 C. T. Johnson, J. A. Wroe, R. Agarwal, K. E. Martin, R. E. Guldberg, R. M. Donland, L. F. Westbladee and A. J. García, *Proc. Natl. Acad. Sci. U. S. A.*, 2018, **115**, E4960.
52 D. Davies, *Nat. Rev. Drug Discovery*, 2003, **2**, 114–122.
53 G. C. Wong and G. A. O'Toole, *MRS Bull.*, 2011, **36**, 339–342.
54 E. M. Hetrick and M. H. Schoenfisch, *Chem. Soc. Rev.*, 2006, **35**, 780–789.
55 J. L. Lister and A. R. Horswill, *Front. Cell. Infect. Microbiol.*, 2014, **4**, 178.
56 M. Riool, L. de Boer, V. Jaspers, C. M. van der Loos, W. J. van Wamel, G. Wu, P. H. S. Kwakman and S. A. J. Zaat, *Acta Biomater.*, 2014, **10**, 5202–5212.
57 J. Ryu, S. H. Ku, H. Lee and C. B. Park, *Adv. Funct. Mater.*, 2010, **20**, 2132–2139.
58 G. K. Toworfe, R. J. Composto, I. M. Shapiro and P. Ducheyne, *Biomaterials*, 2006, **27**, 631–642.
59 K. Shiba, S. Motozuka, T. Yamaguchi, N. Ogawa, Y. Otsuka, K. Ohnuma, T. Kataoka and M. Tagaya, *Cryst. Growth Des.*, 2016, **16**, 1463–1471.
60 E. J. Kwon, M. Skalak, A. Bertucci, G. Braun, F. Ricci, E. Ruoslahti, M. J. Sailor and S. N. Bhatia, *Adv. Mater.*, 2017, **29**, 1701527.
61 G. Wei, J. Reichert, J. Bossert and K. D. Jandt, *Biomacromolecules*, 2008, **9**, 3258–3267.
62 A. Krajewski, M. Mazzocchi, P. L. Buldini, A. Ravaglioli, A. Tinti, P. Taddei and C. Fagnano, *J. Mol. Struct.*, 2005, **744–747**, 221–228.
63 D. A. Hamdi, Z. T. Jiang, K. No, M. M. Rahman, P. C. Lee, L. N. T. Truc, J. Kim, M. Altarawneh, L. Thair, T. A. J. Jumaa and B. Z. Dlugogorski, *Appl. Surf. Sci.*, 2019, **463**, 292–299.